CrossMark

Investigation of Annealing Temperature on Structural and Morphological Properties of Cr_2O_3 Nanoparticles for Humidity Sensor Application

P. Jayamurugan[1] · R. Mariappan[1] · K. Premnazeer[2] ·
S. Ashokan[3] · Y. V. Subba Rao[4] · N. V. S. S. Seshagiri Rao[4] ·
C. Shanmugapriya[5]

Abstract Cr_2O_3 nanoparticles have been prepared for precipitation technique at reaction temperature 50 °C. The prepared samples were annealed different temperatures at 500,700 and 1000 °C. Synthesized powders were characterized as X-ray diffraction, optical, transmission electron microscope, SEM with EDAX, humidity sensor, FTIR. The annealing temperature has been found to be playing a crucial role in the controlling particle size. XRD study shows the rhombohedral crystal structure of highly preferential orientation along (1 0 4) direction. FTIR reveals that the presence Cr–O bonds in the structure. The TEM images show that the size of NPs of Cr_2O_3 varied from 26 to 60 nm with average crystalline size 43 nm. UV–visible spectrum shows the absorption band of Cr_2O_3 nanoparticles at 400 nm. The humidity sensor of the Cr_2O_3 nanoparticles was studied by two temperature method. 1000 °C annealed Cr_2O_3 nanoparticles show better sensing properties and exhibits good linearity in response than 500 °C. SEM images show the clusters and agglomeration of nanoparticles. EDAX spectrum confirms the presence of Cr_2O_3 nanoparticles. Each samples have been characterized as sensing materials to determine relative humidity in the range of 20–90%. The humidity sensing property increased with increasing of annealing temperature and the resistance was decreased.

✉ P. Jayamurugan
    muruganjaya85@gmail.com

[1]   Department of Physics, Adhiyamaan College of Engineering, Hosur, Tamilnadu 635109, India

[2]   Department of Physics, Islamiah College (Autonomous), Newtown, Vaniyambadi,
     Tamil Nadu 635 752, India

[3]   Department of Physics, Bannari Amman Institute of Technology, Sathyamanglam, Erode,
     Tamilnadu 638 401, India

[4]   Department of Physics, Birla Institute of Technology and Science (BITS), Hyderabad Campus,
     Pilani, Hyderabad, Telangana State 500078, India

[5]   Department of Physics, Sona College of Technology, Salem, Tamilnadu, India

1 Introduction

In recent years, metal oxides constitute an important class of materials that are
concerned in environmental science, electrochemistry, biology, chemical sensors,
magnetism and other fields. Among various metal oxides, chromium oxide
(stoichiometric excess of oxygen due to cation vacancies) has drawn much attention
[1–4] because of its unique properties such as high hardness, thermodynamic
stability and resistance to chemical attack and versatile applications such as catalyst
supporter [5], green pigment and protective coating [6], gas sensors [7], etc. [8]. The
sensing response is one of the most important characteristics to be possessed by a
gas sensor. Therefore, it becomes most important to device some techniques to
enhance the sensing response from a gas sensor.

Several sensors based on the ion conducting materials are reported on a variety of
gases [9, 10], SO_x, NO_x, CO_x [11, 12], O_2 [13], H_2O (humidity) [14–17], etc.

Now a days, increased concern about environment protection has led to
continuous expansion in sensor development technology [18]. Especially, sensing
and control of humidity are of great importance in the field of industry, agriculture
and medicine [19].

Particularly, the humidity sensing devices which are widely reported on literature
can be classified into two types of their working principle: (a) impedance type in
which resistance/conductance or capacitance of the sensors changes; and (b) elec-
trochemical cell type in which potential/current changes, due to absorption of water.

In the present work, Cr_2O_3 nanoparticles were synthesized by the chemical
precipitation method. The prepared samples were annealed different temperatures
at, 500, 700 and 1000 °C. Optical, structural, size, humidity sensor and morpho-
logical properties were investigated.

2 Experimental Details

2.1 Synthesis of Chromium Oxide Nanoparticles

Chromium chloride ($CrCl_3 \cdot 6H_2O$) were purchased from Sigma–Alridch, India
Ammonia was obtained from Merck, India.

Nanoparticles of chromium oxide was prepared by following a precipitation
technique.0.2 M solution of $CrCl_3 \cdot 6H_2O$ was dissolved in 100 ml of deionized
water using continuous stirring for 30 min. Then ammonia solution was added to
drop wise with continuous stirring until the pH of the solution reached to 10 for an
hour. After adding ammonia solution,the solution became a white color. The
reaction temperature was maintained at 50 °C using stirrer with hot plate. The
resulting precipitate were separated from solutions. The obtained product was
filtered, washed with deionized water several times and dried into powder at 120 °C

in muffle furnace. After that the sample was naturally allowed to cool to room-temperature by switching off the furnace. The dark green powder was calcined at different temperatures for 500, 700 and 1000 °C for 3 h and it was grinded for an hour. Obtained samplese were found impurity free Cr_2O_3 nanoparticles.

2.2 Humidity Sensing Properties of Cr_2O_3 Nanoparticles

Figure 1 shows experimental set up for humidity sensing properties of Cr_2O_3 nanoparticles. The prepared samples of Cr_2O_3 nanoparticles for 500 and 1000 °C are fine grinded in a mortar and then pressed into pellets using a Pelletizer (»5 MPa). The thickness of the pellets is 3 mm. The top side of the pellet was made contacts two copper wire and silver paste area was 1 mm with the pellet top surface. The prepared pellets are placed inside a dynamic humidity chamber. The humidity system consisted of a closed flask (total volume 500 mL) with two necks for inserting thermometers and the sensor. The flask was partially filled with water and kept in a thermocol container. The external container was filled to the equal level of water with ice. The temperature of the system was adjusted to mixing ice and water as required. Thus, the water inside the flask can be kept at the required temperature (T1). The sensor of Cr_2O_3 nanoparticles pellets were mounted inside the flask at a height of 6 cm from the surface of the water, and the temperature of the sample (T2) was measured with a thermometer placed at an equal height of the sample to be studied. The humidity inside the chamber is calculated by taking the ratio of the saturated water vapor pressure on a water temperature (T1) and the sample temperature (T2). The values of the saturated vapor pressure are obtained from the CRC Handbook of Chemistry and Physics. It should be noted that the temperature of the sample changes from 3–6 °C during the experiment.

Different % RH values are obtained by adjusting the temperature of the water inside the flask, with ice and water mixture from room temperature to 0 °C.
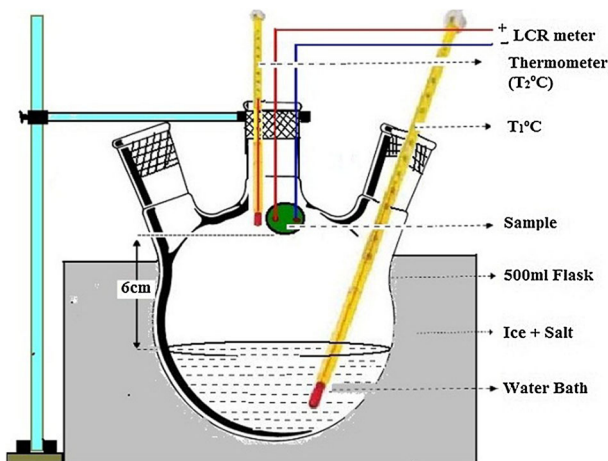

Fig. 1 Schematic experimental set up for the measurement of % RH

The % RH inside the flask is given by following equation [20].

$$\%RH = \frac{Ew(T1)}{Ew(2)} \times 100 \tag{1}$$

where Ew $(T1)$ is the saturated water vapor pressure in the temperature of water and Ew $(T2)$ is the saturated water vapor pressure at the temperature of the sensor element.

Different % RHvalues are obtained by adjusting the temperature of the water inside the flask, with ice and water mixture from room temperature to 0 °C. The system equilibrium was fast and stable readings were obtained within 10 min.

3 Characterization Techniques

TEM images were taken using Hitachi 600 transmission electron microscopy. The morphology and EDAX analysis of the composites was done using a 20 kV JSM-5600 J scanning electron microscopy (SEM). The composition of the films was analyzed by energy dispersive analysis using X-rays (EDAX) equipped in SEM, for which a 20 kV accelerating voltage was applied. The FT-IR spectrum were recorded by using Nicolet Avatar 360 Fourier transform infrared spectrometer with samples dispersed in pressed KBr disks. Optical absorbance spectrum was taken using JASCO V-530 dual beam spectrometer in the wavelength range 200–800 nm with a scanning speed 400 nm/min. The synthesized Cr_2O_3 nanoparticles were then successfully utilized as humidity sensors for a broad range of humidity ranging between 20 and 100% RH using a Fluka 177 digital multimeter with an RS-232 interface by two temperature method.

4 Results and Discussions

4.1 SEM Analysis with EDAX Analysis

Figure 2a–c represents the SEM with EDAX spectrum of the nanostructured Cr_2O_3 powders at various annealing temperatures. Larger numbers of pores are also seen in the pictures Fig. 2a, b.

This higher porosity increases surface to volume ratio which helps in getting good sensitivity. As annealing temperature increases, the pores in the sample increases which results in absorption of more water vapour giving better sensitivity [21].

Figure 2c shows the spherical morphology at a higher calcined temperature for 1000 °C [22].

The higher temperature of Cr_2O_3 nanoparticles show that the pores in the saturated and the condensation of the moisture,which is seen in the Fig. 2c. This leads to the decreases of resistances for Cr_2O_3 nanoparticles. The EDAX spectrum
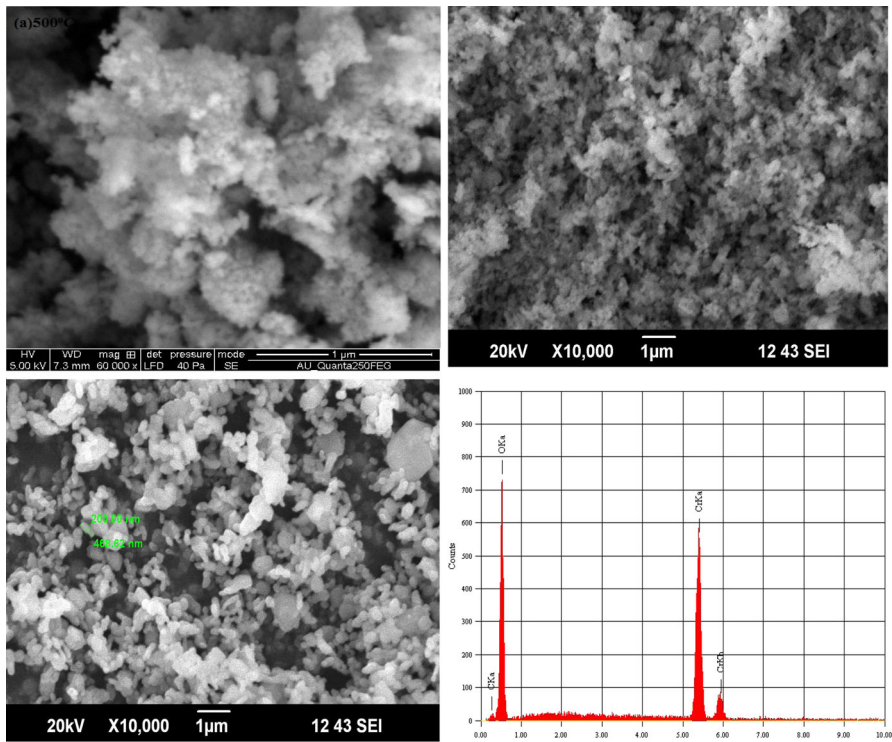
Fig. 2 SEM images of Cr_2O_3 nano particles for 500, 700 and 1000 °C

shows better stoichiometry of the Cr_2O_3 nanoparticles. The elemental composition of the nanostructured Cr_2O_3 powder is presented in Table 1.

4.2 Spectroscopic Analysis

Figure 3 shows the FTIR spectrum of nanostructured Cr_2O_3 powders at various annealing temperatures. A broad band of 3420 cm^{-1} corresponds to the stretching modes of surface OH groups. The band 1033 cm^{-1} is assigned to Cr=O vibrations. Two peaks displayed at 631 and 485.65,510 cm^{-1} attributed to Cr–O stretching modes, are clear evidence for the presence of the crystalline Cr_2O_3 [23, 24].

Table 1 Elemental composition of Cr_2O_3 nanoparticles

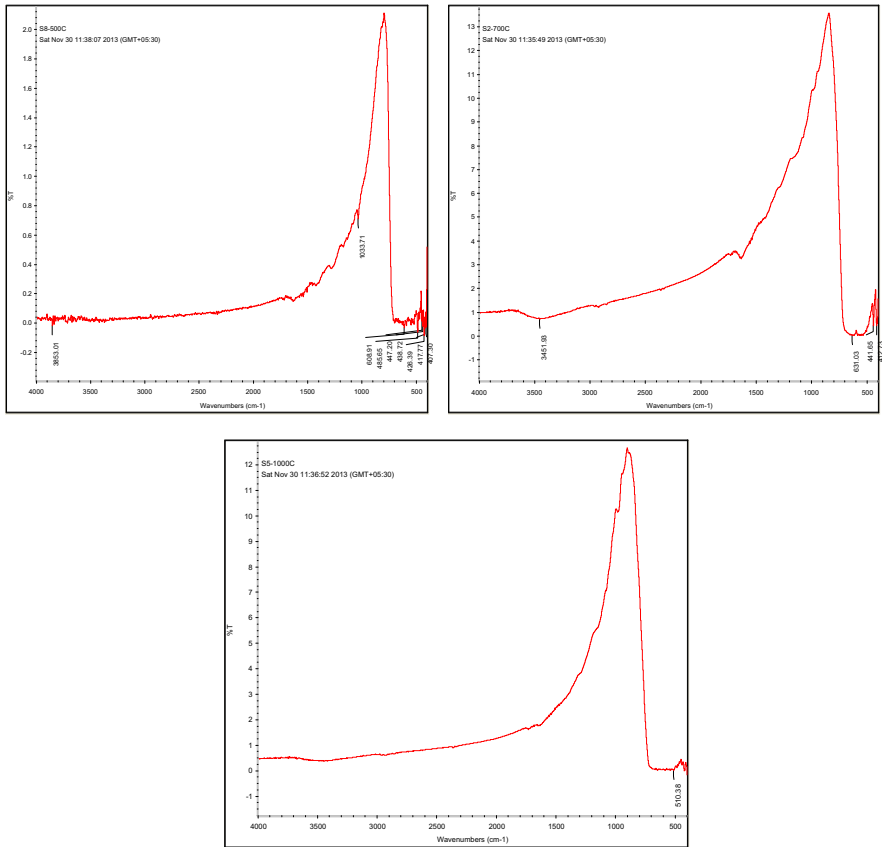| Element	(keV)	Mass (%)	Atom (%)	K
C K	0.277	1.5	3.8	1.4122
O K	0.525	29.48	55.92	0.5373
Cr K	5.411	69.01	40.28	1
Total		100	100	

Fig. 3 FTIR spectra of Cr_2O_3 nano particles for 500, 700 and 1000 °C

4.3 X-ray Diffraction Analysis

The XRD patterns of the Cr_2O_3 nanoparticles prepared for different sintering temperatures (500, 700 and 1000 °C) are shown in Fig. 4. The diffractograms indicate the presence of prominent peaks corresponding to (0 1 2), (1 0 4), (1 1 0), (0 0 6), (1 1 3), (0 2 4), (1 1 6), (2 1 4), (3 0 0), (1 0 10) and (2 2 0) planes of the material from rhombohedral structure. Moreover, the intensity of the peak (104) plane increases with the increase sintering temperature. The comparison was made between the observed diffraction peak patterns with standard diffraction values of JCPDS card no. 84-0315 confirms that the nanoparticles are having rhombohedral crystal structure with highly preferential orientation along (1 0 4) direction. However, [25] have found (1 0 4) as a preferred orientation for their nanoparticles of Cr_2O_3 obtained by. No diffraction peaks of other impurity phases are found in those nanoparticles. The lattice constants 'a' was calculated by using the following expression.
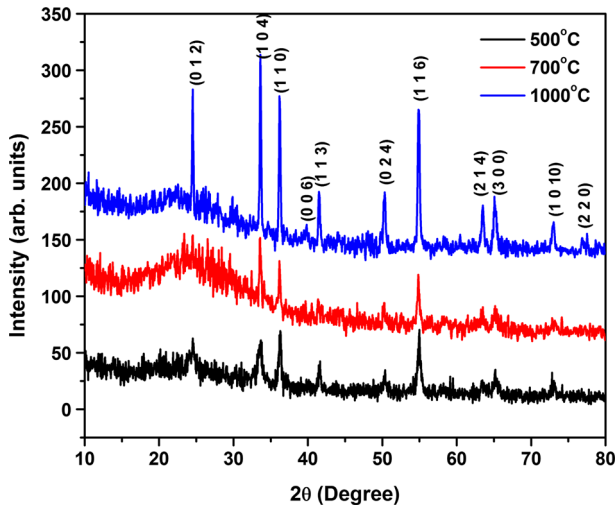
Fig. 4 X-ray diffraction of Cr_2O_3 nano particles for 500, 700 and 1000 °C

$$\frac{1}{d^2} = \left[\frac{1}{a^2} \frac{(h^2 + k^2 + l^2)\sin^2\alpha + 2(hk + kl + lh)(\cos^2\alpha - \cos\alpha)}{1 - 2\cos^3\alpha + 3\cos^2\alpha)} \right] \quad (2)$$

The values of lattice constants 'a' of the Cr_2O_3 nanoparticles are found to be 4.910 for 500 °C and 4.916 for 1000 °C. It is found that the lattice constants 'a' values are in good agreement with the standard values taken from JCPDS data. The XRD was used to calculate the crystallite size (D) with the help of Scherrer's relation.

$$D = \frac{k\lambda}{\beta\cos\theta} \quad (3)$$

where, k is the shape factor usually (k = 0.94), λ is the X-ray wavelength and β is the full width in radian at half maximum of the peak and θ is the Bragg's angle of the X-ray diffraction peak. The crystallite sizes of the all nanoparticles are found to be in the range between 19 and 25 nm for 500 °C and 45–65 nm for 1000 °C. The dislocation density and microstrain were calculated using Eqs. (4) and (5) for the Cr_2O_3 nanoparticles.

$$\delta = \frac{1}{D^2} \, lines/m^2 \quad (4)$$

$$\varepsilon = \frac{\lambda}{D\sin\theta} - \frac{\beta}{\tan\theta} \quad (5)$$

It observed that the dislocation density and micro strain for the (1 0 4) orientation plane decreases in increase of sintering temperature from 500 to 1000 °C and the same may be due to the release of stress in the nanoparticles.

4.4 Optical Properties

Figure 5 shows the optical absorption spectrum of as-grown Cr_2O_3 nanostructures for 500, 700, 1000 °C. In each spectra show the absorption band of 400 nm. This band reveals the absorption band of Cr_2O_3 nanoparticles [26].

4.5 Humidity Sensing Response

The change in relative humidity values are ploted against the corresponding values of resistance and the obtanied humiditity response curve from Cr_2O_3 nanoparticles for 500 and 1000 °C are shown in Fig. 6a, b. 1000 °C shows a linear response from 5% RH to 55% RH. On the other hand, 500 °C Cr_2O_3 nanoparticles, the resistance is found to drop from 5% RH up to 20% RH rapidly in a linear fashion. After 20% RH to decrease to the resistance is very small. the higher calcined temperature Cr_2O_3 reveals there is some change in its resistance with increase in relative humidity. The decrease in resistance is due to the adsorption of water molecules by the surface of the sample. Generally, the humidity sensing property of sample to water vapor can
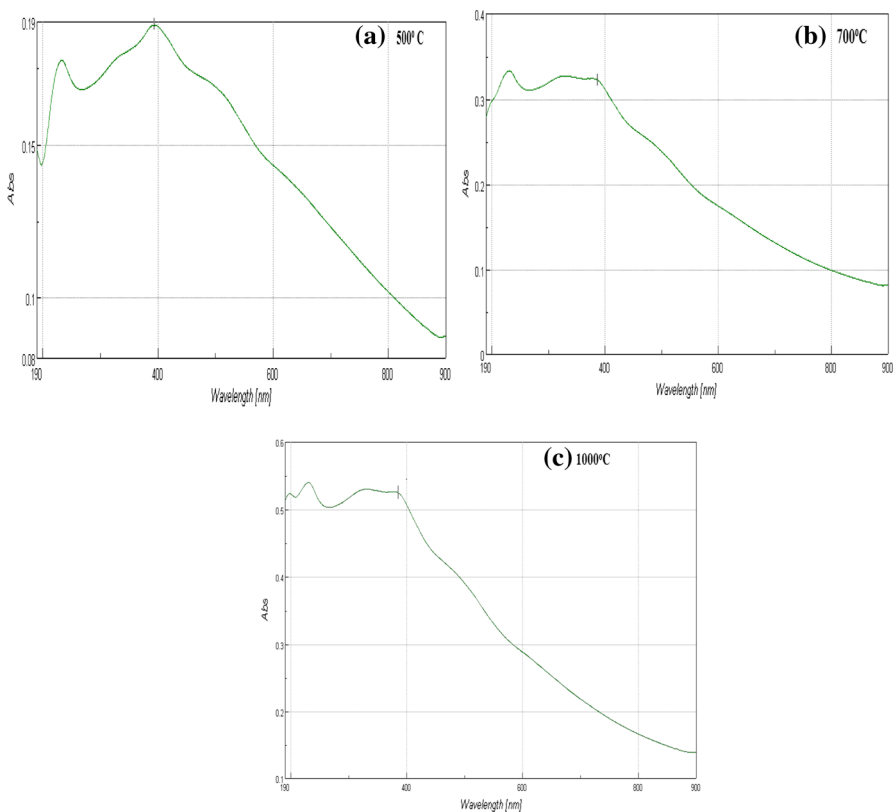
Fig. 5 UV- vis absorption spectrum of Cr_2O_3 nano particles for 500, 700 and 1000 °C
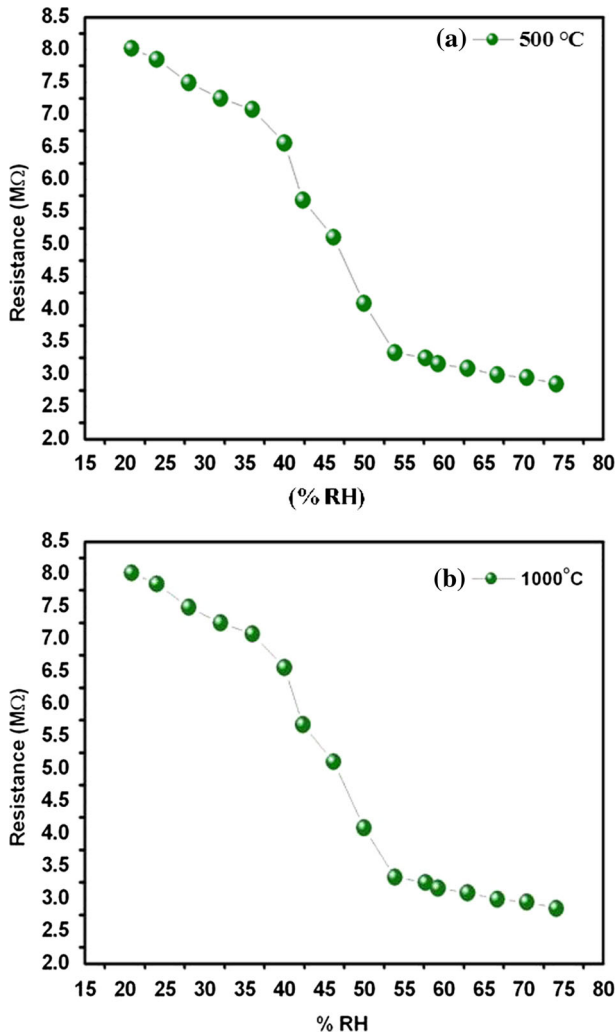
Fig. 6 Variation of resistance with relative humidity for Cr_2O_3 nano particles for **a** 500 °C, and **b** 1000 °C

be regarded as (a) electron hopping assisted by proton transfer mechanism (b) capillary condensation of water molecules into the sample surface [27].

Madhusudhana et al. [28] have studied the variation of resistance with relative humidity(RH) for ZrO2. ZrO2 samples initially the electrical resistance decreases rapidly with a small change in humidity due to adsorption of water vapors. This variation of resistance spectra with humidity implies the different electrical conduction and polarization process that occur in ZrO2 when exposed to the different RH. This high resistance variation in ZrO2 is suitable for lower humidity applications in industries for quick response [29]. In this present work, we have obtained 1000 °C calcined Cr_2O_3 nanoparticles show better sensing in response.

4.6 Transmission Electron Microscopy

TEM images of Cr_2O_3 nanopa rticles are shown in the Fig. 7a–c. The TEM images are indicating that the grain size was homogenous and fairly small (about 26 nm) when the sample was calcined at 500 °C. The sample calcined at 700 °C displayed greater particle size of the enhancement of crystallization or sintering between smaller particles, which is estimated to be about 45 nm. The increase in heat treatment temperature caused the catalyst grains to become larger [30]. The morphology of the prepared Cr_2O_3 nanoparticles calcined at 1000 °C was found to be 60 nm. The TEM images of the prepared Cr_2O_3 nanoparticles indicated that particles present rhomboidal-like morphology and particle size between 25 and 60 nm.
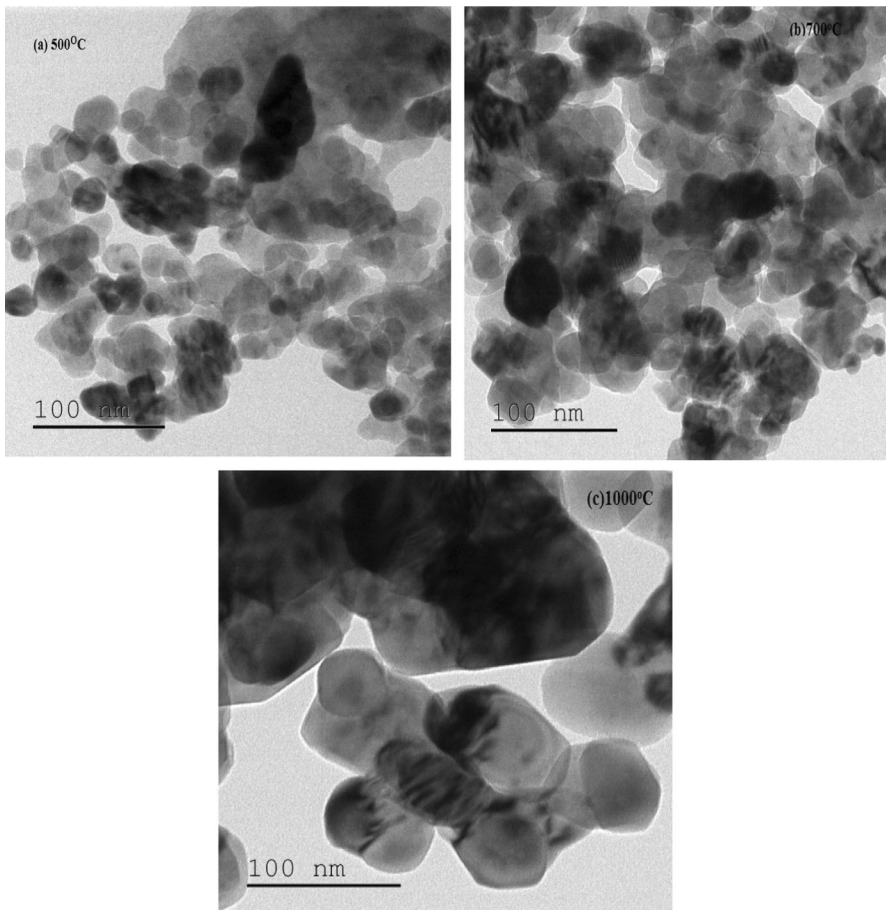

Fig. 7 TEM images of Cr_2O_3 nano particles for 500, 700 and 1000 °C

5 Conclusion

Chromium oxide nanoparticles (NPs) have been rapidly synthesized by precipitation methodusing ammonia as precipitating agent. FTIR spectroscopy, revealed the characteristic peaks of Cr–O bond stretching vibrations. XRD studies show that chromium oxide NP is formed into Cr_2O_3 and it has rhombohedral crystal structure. TEM images shows that the size of NPs of Cr_2O_3 varied from 26 to 60 nm with average crystalline size 43 nm. The spectrum displays the corresponding peaks of chromium and oxygen which clearly reflect that the as-grown material is composed of chromium and oxygen only. The optical study shows absorption spectrum of as-grown Cr_2O_3 nanoparticles. SEM images show pores and spherical morphology in the structure. 1000 °C calcined Cr_2O_3 nanoparticles show better sensing properties and exhibits good linearity in response than 500 °C.

References

1. Suryawanshi, D. N., Patil, D. R., & Patil, L. A. (2008). Fe_2O_3-activated Cr_2O_3 thick films as temperature dependent gas sensors. *Sensors and Actuators B: Chemical, 134,* 579–584.
2. Chabanis, G., Parkin, I. P., & Williams, D. E. (2001). Microspheres of the gas sensor material Cr_2–xTi_xO_3 prepared by the sol–emulsion–gel route. *Journal of Materials Chemistry, 11,* 1651–1655.
3. An, G., Zhang, Y., Liu, Z., Miao, Z., Han, B., Miao, S., et al. (2008). Preparation of porous chromium oxide nanotubes using carbon nanotubes as templates and their application as an ethanol sensor. *Nanotechnology, 19,* 035504.
4. Singh, R. C., Kohli, N., Singh, M. P., & Singh, O. (2010). Ethanol and LPG sensing characteristics of SnO_2 activated Cr_2O_3 thick film sensor. *Bulletin of Materials Science, 33,* 575–579.
5. Weckhuysen, B. M., & Schoonheydt, R. A. (1999). Alkane dehydrogenation over supported chromium oxide catalysts. *Catalysis Today, 51,* 223–232.
6. Ku, R. C., & Winterbottom, W. L. (1985). Electrical conductivity in sputter-deposited chromium oxide coatings. *Thin Solid Films, 127,* 241–256.
7. Miremadi, B. K., Singh, R. C., Chen, Z., Morrison, S. R., & Colbow, K. (1994). Chromium oxide gas sensors for the detection of hydrogen, oxygen and nitrogen oxide. *Sensors and Actuators B: Chemical, 21,* 1–4.
8. Takeda, Y., Kanno, R., Tsuji, Y., Yamamoto, O., & Taguch, H. (1983). Chromium oxides as cathodes for lithium cells. *Journal of Power Sources, 9,* 325–328.
9. Schoonman, J., & Kiliaan, H. S. (1983). In-situ storage of solar hydrogen in a PEC cell. *Solid State Ionics, 9–10,* 1087–1092.
10. Miura, N., Kato, H., Yamazoe, N., & Seiyama, T. (1983). An improved type of proton conductor sensor sensitive to H_2 and CO at room temperature. *Chemistry Letters, 10,* 1573–1576.
11. Gauthier, M., & Chamberland, A. (1977). Solid-state detectors for the potentiometric determination of gaseous oxides I. Measurement in air. *Journal of the Electrochemical Society, 124,* 1579–1583.
12. Lu, G., Miura, N., & Yamazoe, N. (2000). Stabilized zirconia-based sensors using WO_3 electrode for detection of NO or NO_2. *Sensors and Actuators B: Chemical, 65,* 125–127.
13. Xu, Y., Zhou, X., & Sorensen, O. T. (2000). Oxygen sensors based on semiconducting metal oxides: An overview. *Sensors and Actuators B: Chemical, 65,* 2–4.
14. Deniard-Courant, S., Piffard, Y., Barbour, P., & Linage, J. (1988). Relative humidity influence on the water content and on the protonic conductivity of the phosphatoantimonic acids $HnSbP_2O_3n + 5$, xH_2O (n = 1, 3, 5). *Solid State Ionics, 27,* 189–194.
15. Chandra, S., & Hashmi, S. A. (1990). Humidity sensor using a proton conductor ammonium para-tungstate pentahydrate ($APT \cdot 5H_2O$). *Solid State Ionics, 40–41,* 460–462.

16. Iwahara, H., Uchida, H., & Kondo, J. (1983). Galvanic cell-type humidity sensor using high temperature-type proton conductive solid electrolyte. *Journal of Applied Electrochemistry, 13,* 365–370.
17. Miyazaki, K., Xu, C. N., & Haeda, M. (1994). A new potential-type humidity sensor using EMD-based manganese oxides as a solid electrolyte. *Journal of the Electrochemical Society, 141,* L35.
18. Park, S., & King, J. (2001). One-bodied humidity and temperature sensor having advanced linearity at low and high relative humidity range. *Sensors and Actuators B: Chemical, 76,* 322–326.
19. Ramaprasad, A. T., & Rao, V. (2010). Chitin–polyaniline blend as humidity sensor. *Sensors and Actuators B: Chemical, B148,* 117–125.
20. Kulkarni, M. V., & Viswanath, A. K. (2005). Spectroscopic, thermal and electrical properties of sulphonic acids doped poly (o-anisidine) and their application as humidity sensor. *Sensors and Actuators B: Chemical, 107,* 791–797.
21. Rama, S., & Avadhesh Kumar, Y. (2011). Synthesis and humidity sensing investigations of nanostructured $ZnSnO_3$. *Journal of Sensor Technology, 1,* 116–124.
22. Sangeetha, S., Basha, R., Sreerama, K. J., Sangilimuthu, S. N., & Nair, B. U. (2012). Functional pigments from chromium (III) oxide nanoparticles. *Dyes and Pigments, 94,* 548–552.
23. Henderson, M. A. (2010). Photochemistry of methyl bromide on the α-Cr_2O_3 (0001) surface. *Surface Science, 604,* 1800–1807.
24. Rakesh, Ananda, S., & Gowda, N. M. M. (2013). Synthesis of chromium (III) oxide nanoparticles by electrochemical method and Mukia Maderaspatana plant extract, characterization, $KMnO_4$ decomposition and antibacterial study. *Modern Research in Catalysis, 2,* 127–135.
25. Hassen, A., El-Sayed, S., Morsi, W. M., & El Sayed, A. M. (2014). Preparation, dielectric and optical properties of Cr_2O_3/PVC nanocomposite films. *Journal of Advances in Physics, 4,* 571–584.
26. Jaswal, V. S., Arora, A. K., Kinger, M., & Gupta, V. D. (2014). Synthesis and characterization of chromium oxide nanoparticles. *Oriental Journal of Chemistry, 30*(2014), 559–566.
27. Faia, M., Furtado, C. S., & Ferreira, A. J. (2005). AC impedance spectroscopy: A new equivalent circuit for titania thick film humidity sensors. *Sensors and Actuators B: Chemical, 107,* 353–359.
28. Madhusudhanaa, H. C., Shobhadevic, S. N., Nagabhushanad, B. M., Chaluvarajue, B. V., Murugendrappaf, M. V., Hari Krishnad, R., et al. (2016). Effect of fuels on conductivity, dielectric and humidity sensingproperties of ZrO_2 nanocrystals prepared by low temperature solutioncombustion method. *Journal of Asian Ceramic Societies, 4,* 309–318.
29. Wang, Z., Lu, Y., Yuan, S., Shi, L., Zhao, Y., Zhang, M., et al. (2013). Hydrothermal synthesis and humidity sensing properties of size-controlled zirconium oxide (ZrO_2) nanorods. *Journal of Colloid and Interface Science, 396,* 9–15.
30. Bhosale, R., Pujari, S., Muley, G., Pagare, B., & Gambhire, A. (2013). Visible-light-activated nanocomposite photocatalyst of Cr_2O_3/SnO_2. *Journal of Nanostructure in Chemistry, 3,* 46.